Solid State Communications 151 (2011) 1851–1855

Contents lists available at SciVerse ScienceDirect

Solid State Communications

journal homepage: www.elsevier.com/locate/ssc

Fast-track communication

Meeting experimental challenges to physics of network glasses: Assessing the role of sample homogeneity

S. Bhosle [a], K. Gunasekera [a], Ping Chen [a,1], P. Boolchand [a,*], M. Micoulaut [b], C. Massobrio [c]

[a] School of Electronic & Computing Systems, College of Engineering and Applied Science, University of Cincinnati, Cincinnati, OH 45221-0030, United States
[b] Laboratoire de Physique Theorique de la Matiere Condensee, Universite Pierre et Marie Curie, Boite 121, 4 Place Jussieu, 75252 Paris Cedex 05, France
[c] Institut de Physique et de Chimie des Materiaux de Strasbourg, 23 rue du Loess, BP43, F-67034 Strasbourg Cedex 2, France

ARTICLE INFO

Article history:
Received 15 September 2011
Received in revised form
12 October 2011
Accepted 13 October 2011
by A. Pinczuk
Available online 20 October 2011

Keywords:
A. Chalcogenide glasses
D. Self-organization
E. Raman scattering
E. Modulated DSC

ABSTRACT

We introduce a Raman profiling method to track homogenization of Ge_xSe_{100-x} melts in real time, and show that 2 g melts reacted at 950 °C in high vacuum homogenize in 168 h on a scale of 10μm. Homogenization of melts is precursive to self-organization of glasses. In the present glasses, compositional variation of Raman active corner-sharing mode frequency of $GeSe_4$ units, molar volumes, and the enthalpy of relaxation at T_g, reveal the rigidity ($x_c(1) = 19.5(3)\%$) and the stress ($x_c(2) = 26.0(3)\%$) transitions to be rather sharp ($\Delta x < 0.6\%$). These abrupt elastic phase transitions are in harmony with rigidity theory and have a direct bearing on the physics of glasses.

1. Introduction

Bulk glasses have been synthesized by reacting starting materials to produce melts, which are then quenched to produce disordered solids [1]. One generally assumes that holding melts at several hundred degrees above the liquidus for several hours would homogenize them. In equilibrium phase diagrams, glass forming compositions are usually bordered by congruently melting crystalline phases [2]. These crystalline phases, in principle, can nucleate as melts are quenched to produce microscopic heterogeneities (MH). In practice, such equilibrium thermodynamic effects can be suppressed in *pure* melts as heterogeneous nucleation sites become minuscule as shown recently in metallic glasses [3]. We introduce here a Raman profiling method to track the homogenization of chalcogenides melts in real time, and find that the process consists of two steps, an initial *step* 1 as starting materials react to produce MH consisting of crystalline phases embedded in a glass. Continued reaction leads the crystalline phases to dissolve and local structures characteristic of melts/glasses to emerge. In *step* 2, intermediate and extended range structures evolve as melt stoichiometry across a batch composition equalizes by a process that can be described as Melt-Nanoscale Mixing (MNM). We illustrate these ideas for the case of the well studied Ge_xSe_{100-x} binary [4–14], and find that *slow* MNM and not MH due to thermodynamic phase separation [15] is the determinative factor that contributes to heterogeneity of chalcogenide glasses.

The finding has a direct bearing on the sharpness of the *rigidity* and *stress* transitions in the Ge_xSe_{100-x} binary glasses. Rigidity theory [16–18] has been the corner stone to understanding network glasses in terms of their topology. An intermediate phase (IP) forms between these transitions [19] and has attracted widespread interest because of its exceptional functionalities, including the stress-free, non-aging, dynamically reversible nature of networks formed in this nanostructured phase [8,9,18,20,21]. In the present homogenized glasses, we find the rigidity and stress transitions to occur near $x = 19.5(3)\%$ (*rigidity*) and 26.0(3)% (*stress*) and to be rather *sharp* (width $\Delta x < 0.6\%$). Our findings illustrate that the intrinsic stress-driven behavior of these chalcogenide glasses may be far richer than hitherto recognized. The Raman profiling method provides a powerful means to access homogeneous glasses and melts to explore their intrinsic nanostructure.

2. Experimental

Elemental Ge and Se lumps (3–4 mm diam.) of 99.999% purity from Cerac Inc, encapsulated in 5 mm ID quartz tubing at 1×10^{-7} Torr, were reacted at 950 °C for periods, t_R, ranging from $6\,h < t_R < 168\,h$ in a T-regulated box furnace, with tubes held vertically. Batch sizes were kept near 2 g. Quartz tubings were washed

* Corresponding author.
E-mail address: boolchp@ucmail.uc.edu (P. Boolchand).
[1] Current address: Department of Electrical & Computer Engineering, Boise State University, Boise ID 83725, United States.

0038-1098/$ – see front matter © 2011 Elsevier Ltd. All rights reserved.
doi:10.1016/j.ssc.2011.10.016

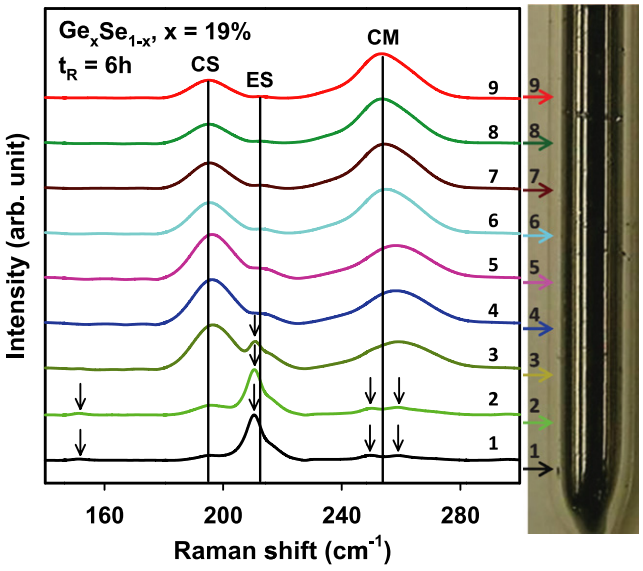

Fig. 1. (Color online) Raman scattering of quenched $Ge_{19}Se_{81}$ melt taken along the quartz tube length at 9 locations, 6 h after reacting the starting materials at 950 °C. The spacing between successive points along the quartz tube is about 2.5 mm. The sharp modes at the arrow locations are those of 2D or α-$GeSe_2$. CS = Corner Sharing, ES = Edge Sharing and CM = Chain mode.

using Ammonium bifluoride followed by a rinse in de-ionized water and rapid drying. Prior to use quartz tubing was dried in a vacuum oven (90 °C) for 24 h. Periodically, melt temperatures were lowered to 50 °C above liquidus [2] and water quenched, and examined in FT-Raman profiling experiments. These measurements used 1.064 μm radiation from a Nd-YAG laser with a 50 μm spot size to excite the scattering, and spectra were acquired along the 1 inch length of a glass column at 9 locations (Fig. 1). In the initial stages of alloying (t_R = 6 h), melts are, indeed, quite heterogeneous as revealed by significant changes in the Raman spectra from point 1 to 9. The 9 Raman lineshapes are superimposed in Fig. 2a, and provide a pictorial view of melt heterogeneity. Continued reaction (t_R = 96 h) of melts, promotes homogeneity (Fig. 2c), but a fully homogeneous melt is realized only after t_R = 168 h (Fig. 2d) when all 9 line shapes *coalesce*. We have synthesized 21 glass compositions in the 10% < x < 33.33% range, and ascertained their homogeneity by Raman profiling scans in each case [22]. Once homogenized, an additional profiling experiment using a micro-Raman dispersive system (Model T64000 system from Horiba Inc) with a 10 μm laser spot size was performed and samples were found to be reasonably well homogenized on that finer scale as well [22]. Separately, we also synthesized glasses at x = 19% and 33.33% using finely crushed Ge and Se powders stored at laboratory ambient (45% rel. humidity) as starting materials. These melts reacted quicker in the first step (t_R < 48 h) but took as much time (t_R = 96 h) as others to nanoscale mix in Step 2. However, their structural properties are measurably different [22] from their dry counterparts and are characteristic of wet samples containing hydrolyzed products (see below). The final step in synthesis was to thermally cycle all quenched melts through T_g. This was achieved by heating quartz tubes containing quenched melts to T_g in a box furnace, and slow cooling to room temperature at 3 °C/min to realize bulk glasses with a common thermal history at various compositions.

3. Results and discussion

In Step 1 of reaction of a melt at x = 19%, MH are clearly manifested as α-$GeSe_2$ [6] fragments nucleate in the glass at the tube bottom, and the evidence consists of the narrow modes (arrows)

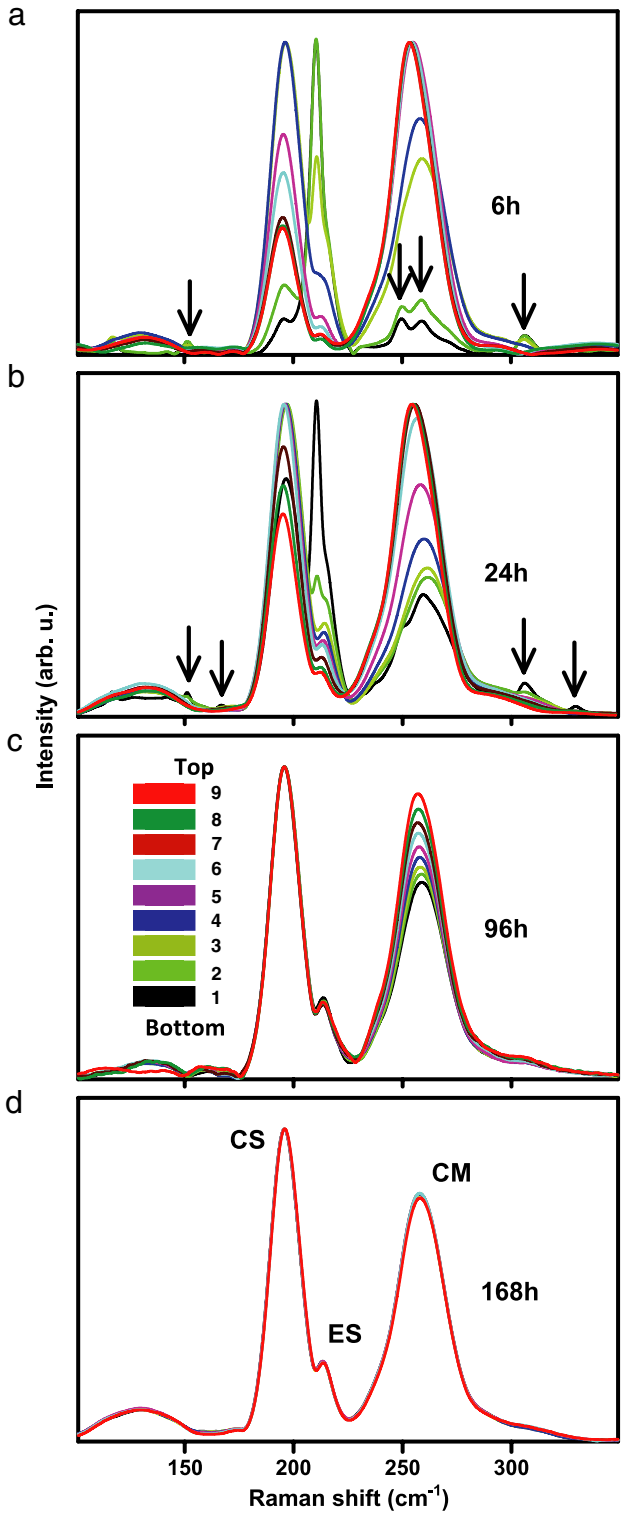

Fig. 2. (Color online) A coalesced view of the 9 Raman spectra of Fig. 1 appears in panel (a). Prolonged reaction of the $Ge_{19}Se_{81}$ melt for (b) 24 h, (c) 96 h, (d) 168 h (d) show it homogenizing. In (c), we provide the color/location key of Fig. 1.

observed at locations 1, 2, and 3 in Figs. 1, and 2a and b. At point 4 in Fig. 1, a binary glass of $Ge_{19}Se_{81}$ stoichiometry forms, and as one approaches the top (point 9) of the column, melts become steadily Ge-deficient (Ge_8Se_{92}), as estimated from the increased scattering strength ratio of the chain-mode (CM, near 250 cm^{-1}) to $GeSe_4$ corner-sharing mode (CS, near 200 cm^{-1}) [6,7]. With increasing t_R > 24 h the crystalline phase dissolves in the glassy matrix. At

t_R = 96 h, the crystalline phase completely vanishes, but a heterogeneous melt persists (Fig. 2c) with Ge content 'x' varying almost linearly from 21% at location 1% to 17% at location 9 along the length of the column. In the spectra, the absence in the spatial variation of the CS mode strength is due to normalizing the spectra to that mode. At this point appropriate local structures characteristic of melts/glasses have evolved but the glass is heterogeneous. A further reaction of the melt to t_R = 168 h leads to the Ge content across the batch composition to equalize, and a fully homogeneous glass on a scale of 10 μm is realized. The 2-step behavior of homogenization of melts reported here at x = 19% is observed at all other compositions examined in the present Ge_xSe_{100-x} binary [22]. Heterogeneity of glasses in calorimetric measurements could only be established if one were to map T_gs across a batch composition, which is an insurmountable task. Our experiments also reveal that rocking the reaction tube speeds up Step 1 of the homogenization, but it is Step 2 of MNM that is the rate limiting process to melt homogenization. MNM requires a large number of correlated sequential bond-breaking and bond-forming steps for the 4-fold coordinated Ge to diffuse, and the Ge/Se ratio across a batch to equalize. Separately, 1/4 g sized melts were also studied, and found to homogenize in 6 h rather than 168 h needed for the 2 g batch size [22]. The result is the consequence of a 5-fold reduction in diffusion length for Ge and Se atoms to move across as concentration gradients vanish. From these data, we obtain a diffusion constant for Ge and Se atoms in Ge_xSe_{100-x} melts at 950 °C of $D = 4 \times 10^{-6}$ cm^2/s.

Raman scattering of bulk glasses encapsulated in quartz tubings were then examined in the dispersive system but in a macro-mode (to suppress light-induced effects) using 5 mW of 647 nm radiation with a 50 μm laser spot size. The observed lineshapes were least-squares fit [7] to the superposition of Gaussians, and the variation in the CS mode frequency ($\nu_{CS}(x)$) was deduced (Fig. 3a). These data show three distinct regimes of variation, a power-law behavior at $x > 26.0\%$, an approximately linear variation in the $19.5\% < x < 26\%$ range, and again a linear variation but with a higher slope at $x < 19\%$. Density of glasses could be measured using a quartz fiber with a digital balance and dry alcohol to 1/4% accuracy with large samples [22]. The variation of molar volumes ($V_m(x)$) with composition (Fig. 3b) on dry glasses also show [22] three distinct regimes- a nearly flat regime in the $19.5\% < x < 26\%$ range, and a rapid rise at $x > 26\%$ and at $x < 19\%$, with the two thresholds coinciding with the Raman $\nu_{CS}(x)$ trends. Glass transition temperatures, $T_g(x)$, the jump in the specific heat at T_g ($\Delta C_p(x)$) and the relaxation enthalpy at T_g ($\Delta H_{nr}(x)$) [7], were also measured using a model 2920 modulated DSC from TA Instruments, and some of these data appear in Fig. 3a and c. The smooth line through the $T_g(x)$ data represents a plot of the polynomial, $T_g(x) = 39.781 + 8.702x - 0.271x^2 + 0.11x^3$, and fits the data within 2 °C except near the inflexion point ($x_c(3) = 31.5\%$). Near the inflexion point, dT_g/dx was deduced by averaging the slope using 4 adjacent data points, and we find the slope to maximize near $x = x_c(3)$, and to vanish when T_g maximizes near $x = 33.3\%$ as expected.

The observed CS mode frequency variation, $\nu_{CS}(x)$ (Fig. 3a), serves to uniquely identify the phase formed at $x > 26\%$ to be the *stressed-rigid* phase [7]. We have extracted the underlying optical elasticity (which varies as ν_{CS}^2) power-law variation in x, using Eq. (1)

$$\nu_{CS}^2(x) - \nu_{CS}^2(x_c(2)) = A(x - x_c(2))^{p_2}. \quad (1)$$

Here $\nu_{CS}^2(x_c(2))$ represents the value of $\nu_{CS}^2(x)$ at the threshold composition, $x = x_c(2)$, and p_2 the elastic power law in the *stressed-rigid* regime. The data at $x > 26\%$ (Fig. 3a) was used to extract p_2, this time by an *iterative process* using [22] both a polynomial fit and separately a log–log fit to (1). The value of

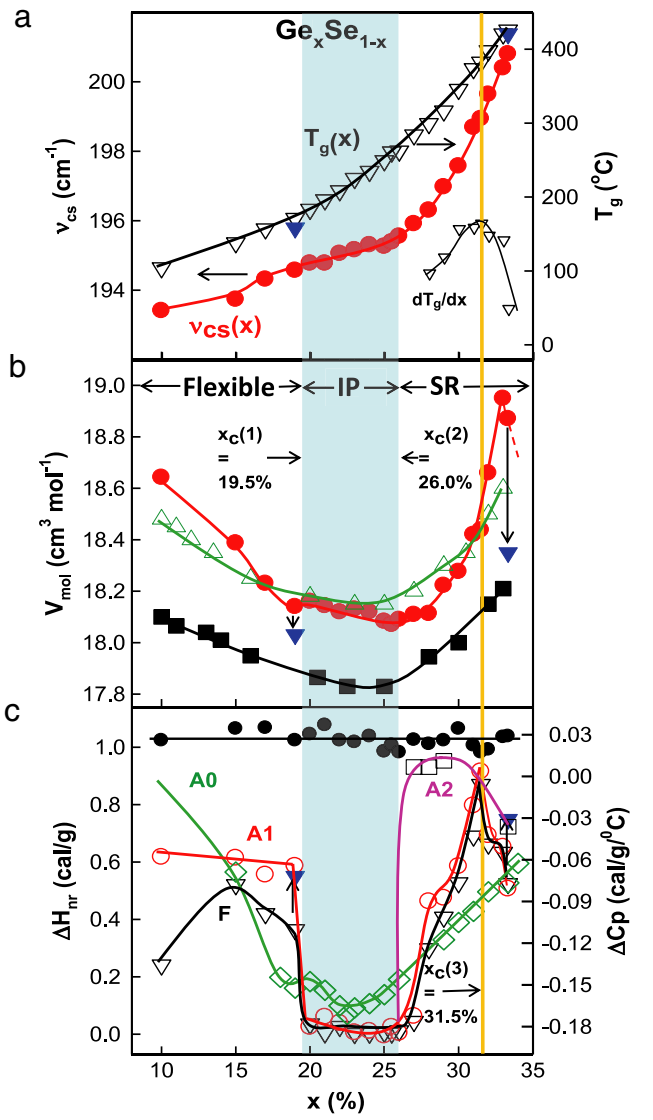

Fig. 3. (Color online) Compositional trends of (a) $T_g(x)$ (▽) and CS mode frequency $\nu(x)$ (●), (b) molar volumes results from present work (●), from Ref. [5] (■) and from Ref. [4] (△), (c) variation in $\Delta C_p(x)$ (●) shows the lack of a dependence on x in the range examined. Variations in non-reversing enthalpy at T_g, $\Delta H_{nr}(x)$, in present samples in fresh (F) state (▽), after 2 weeks of aging at 25 °C (○) curve **A1**, after 2 weeks of aging at 240 °C (□) curve **A2**, and results from Ref. [7] (◊) curve **A0** after 2 weeks of aging at 25 °C. The shaded panel gives the intermediate phase. The ▼ data points in the three panels correspond to wet samples. See text.

$x_c(2)$ was varied so that both fitting procedures yielded the same p_2, and the final result (Fig. 4a) gives $p_2 = 1.50(3)$ and $x_c(2) = 26.0(3)$. The value of p_2 is in excellent agreement with a numerical simulation of the power-law [23]. For the IP, a similar procedure gives (Fig. 4b) $x_c(1) = 19.5(3)\%$ and $p_1 = 1.10(5)$. The present value of p_1 is larger and more accurate than our previous report [19] and its magnitude almost identical to values noted earlier in IPs of modified oxides [24] and chalcogenides [25].

Most striking is the sharpening of the *rigidity* and *stress* transitions upon *aging* of samples. The $\Delta H_{nr}(x)$ results on fresh samples (curve *F*, Fig. 3c) become *step-like* near $x = 19.5\%$ after 2 weeks of aging at room temperature (T_{aging} = 23 °C) (curve A1, Fig. 3c). The use of a higher T_{aging} = 240 °C for stressed-rigid glasses (because of their higher T_g) also leads to a striking *step-like* increase of $\Delta H_{nr}(x)$ term near the stress-transition (curve A2, Fig. 3c). These data are in harmony with the percolative nature of these elastic phase transitions predicted by the pebble game [17].

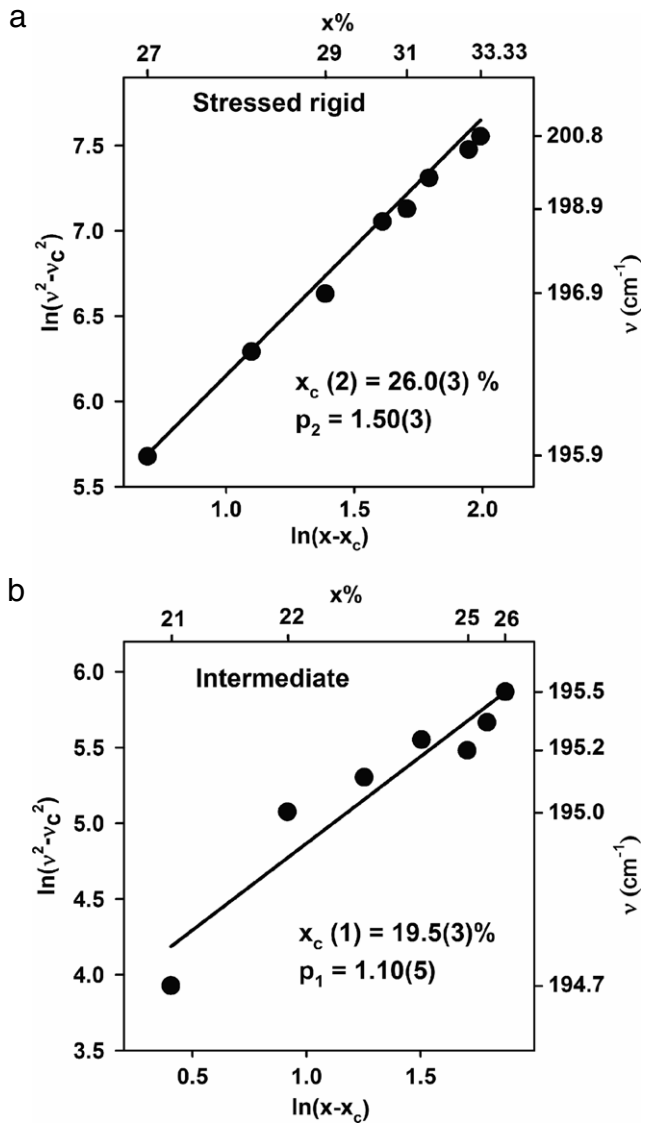

Fig. 4. Elastic threshold compositions (x_c) and optical elastic power-laws (p) in (a) stressed-rigid and (b) intermediate phase deduced from the fitting the Raman mode frequency, $\nu_{CS}(x)$, to Eq. (1).

The vanishing of $\Delta H_{nr}(x)$ term in the IP is entirely consistent with the strict isostaticity of networks formed in that phase [26]. These A1 and A2 data sets on *aged* samples must be compared with the triangular variation of $\Delta H_{nr}(x)$ observed on 2-week aged samples (curve A0, Fig. 3c) reported in Ref. [7]. We can now estimate the spread in Ge stoichiometry of glasses of Ref. [7] to be + or −2% in x from the known heat treatment of melts. For the composition close to the reversibility window center, $x \sim 23\%$, one expects both data sets (A0 and A1) to show the $\Delta H_{nr}(x)$ term to vanish, as they indeed do. However, as one goes away from the center, the $\Delta H_{nr}(x)$ term should increase linearly in the heterogeneous samples (of Ref. 7) as contributions to the heat flow term from the flexible (stressed-rigid) phase steadily weigh in on the low (high) x side. Thus, one can naturally understand how square-well like variation of $\Delta H_{nr}(x)$ in the present very homogeneous samples translates into an almost triangular (Fig. 3c) variation of $\Delta H_{nr}(x)$ in the heterogeneous ones of Ref. [7]. Flexible and stressed-rigid structures compact upon aging and lower the entropy of a glass as found at $x < 20\%$ and at $x > 26\%$, and lead the ΔH_{nr} term to increase. Some sharpening of the *rigidity* and *stress* transitions upon aging is a natural consequence of compositions outside the IP aging but not those in the IP.

Of more than passing interest is the jump in specific heat $\Delta C_p(x) = 0.029(5)$ cal/g/°C deduced from the reversing heat flow that is almost independent of x in the present homogeneous glasses (Fig. 3c). A value of of $\Delta C_p(x) = 0.028(5)$ cal/g/°C was also noted in the $Ge_xAs_xSe_{100-2x}$ ternary [27] over a wide range $0.06 < x < 0.23$ encompassing the IP. In the present binary [28] and the $Ge_xAs_xSe_{100-2x}$ ternary [29], the fragility of melts shows a global minimum for IP compositions. Thus, it appears that in chalcogenides the fragile-strong classification of melts ($T > T_g$) [30] based on dynamics (viscosity) correlates far better with the non-ergodic enthalpy of relaxation $\Delta H_{nr}(x)$ than with the ergodic $\Delta C_p(x)$ (Fig. 3c) in glasses ($T < T_g$).

Traces of bonded water in chalcogenide glasses will lead their physical properties to change measurably compared to their dry counterparts. Some of the bridging Se sites (≡ Ge–Se–Ge ≡) are replaced by ≡ Ge–OH···H–Se–Ge ≡ signatures, thus cleaving (....) the network and creating dangling ends (OH, H). The presence of dangling ends lowers network connectivity, which is reflected in T_g of a dry glass ($x = 19\%$) of 170.8(2.0) °C decreasing to 156.6(2.0) °C for a wet one. Cleaving a network, in general, leads to better packing, and that is reflected in the molar volume of a dry glass ($x = 19\%$) of 18.34(4) cm^3 reducing to 18.03(4) cm^3 (Fig. 3b) for a wet one. The $\Delta H_{nr}(x)$ term in a wet glass at $x = 19\%$ of 0.55(5) cal/g is greater than for its dry counterpart of 0.36(5) cal/g; the result reflects the opening [22] of a new degree of freedom due to dangling ends as additional heat can now be absorbed upon heating to T_g. Closely parallel results due to bonded water are found at other compositions ($x = 33.33\%$ (Fig. 3)). Compositional trends in molar volumes, $V_m(x)$ (Fig. 3b), suggest that glass samples of Ref. [5] are most likely not as dry as those of Ref. [4], while those of Ref. [4] are not as homogeneous as the present ones. These observations highlight the need to seal the pure and dry starting materials as lumps in quartz tubes under high vacuum ($<10^{-7}$ Torr) to suppress bonded water related effects, and to homogenize melts by an adequate heat treatment followed by T_g cycling to access the intrinsic physical behavior of pure and homogeneous bulk glasses.

The nature of the sharp threshold observed near the composition $x_c(3) = 31.5\%$ (Fig. 3) deserves a final comment. In Raman scattering, Ge–Ge bonds as part of ethane-like units [10] first manifest near $x = x_c(3) = 31.5\%$. The cusp in $\Delta H_{nr}(x)$ (Fig. 3c) coincides with a maximum in the slope dT_g/dx (Fig. 3a). Both these observables are related to the network topology [31]. And we understand the reduction in $\Delta H_{nr}(x)$ and in dT_g/dx at $x > 31.5\%$ as due to the decoupling [10] of ethanelike units from the backbone. The nanoscale phase separation leads to a maximum [10] of T_g near $x = 33.33\%$.

4. Conclusions

A Raman profiling method is introduced. It has permitted the synthesis of bulk Ge_xSe_{100-x} glasses of unprecedented homogeneity, resulting in well defined rigidity and stress transitions, in harmony with rigidity theory. Differences in physical behavior of glasses in the Intermediate phase from those outside that phase are accentuated in *homogeneous* glasses. These considerations will apply generally to other chalcogenide glasses. Melt homogenization on a scale of 10 μm appears sufficient to promote self-organization of chalcogenide glasses, and opens a new avenue to experimentally access the *intrinsic* physical behavior of these fascinating materials, both in the glassy ($T < T_g$) and the liquid [32–34] state ($T > T_g$).

Acknowledgments

We thank J.C. Phillips, D. McDaniel, L. Thomas, B. Goodman, and B. Zuk for discussions during the course of this work. This work is supported by NSF grant DMR 08-53957.

References

[1] R. Zallen, The Physics of Amorphous Solids, Wiley, New York, 1983.
[2] H. Ipser, M. Gambino, W. Schuster, Monatshefte für Chemie/Chemical Monthly 113 (1982) 389–398.
[3] T. Yamamoto, N. Yodoshi, T. Bitoh, A. Makino, A. Inoue, Reviews on Advanced Materials Science 18 (2008) 126–130.
[4] S. Mahadevan, A. Giridhar, A.K. Singh, Journal of Non-Crystalline Solids 57 (1983) 423–430.
[5] A. Feltz, H. Aust, Blayer, Journal of Non-Crystalline Solids 55 (1983) 179–190.
[6] Y. Wang, M. Nakamura, O. Matsuda, K. Murase, Journal of Non-Crystalline Solids 266–269 (2000) 872–875.
[7] X.W. Feng, W.J. Bresser, P. Boolchand, Physical Review Letters 78 (1997) 4422–4425.
[8] G. Chen, F. Inam, D.A. Drabold, Applied Physics Letters 97 (2010) 131901–131903.
[9] C. Massobrio, M. Celino, P.S. Salmon, R.A. Martin, M. Micoulaut, A. Pasquarello, Physical Review B 79 (2009) 174201.
[10] P. Boolchand, W.J. Bresser, Philosophical Magazine B 80 (2000) 1757–1772.
[11] E.L. Gjersing, S. Sen, B.G. Aitken, The Journal of Physical Chemistry C 114 (2010) 8601–8608.
[12] F. Inam, G. Chen, D.N. Tafen, D.A. Drabold, Physica Status Solidi B–Basic Solid State Physics 246 (2009) 1849–1853.
[13] P.S. Salmon, Journal of Non-Crystalline Solids 353 (2007) 2959–2974.
[14] I. Petri, P.S. Salmon, H.E. Fischer, Physical Review Letters 84 (2000) 2413–2416.
[15] P. Lucas, E.A. King, O. Gulbiten, J.L. Yarger, E. Soignard, B. Bureau, Physical Review B 80 (2009) 214114.
[16] J.C. Phillips, Journal of Non-Crystalline Solids 34 (1979) 153–181.
[17] M.F. Thorpe, D.J. Jacobs, M.V. Chubynsky, J.C. Phillips, Journal of Non-Crystalline Solids 266 (2000) 859–866.
[18] M. Micoulaut, J.C. Phillips, Physical Review B 67 (2003) 104204–104209.
[19] P. Boolchand, X. Feng, W.J. Bresser, Journal of Non-Crystalline Solids 293 (2001) 348–356.
[20] M.A. Brière, M.V. Chubynsky, N. Mousseau, Physical Review E 75 (2007) 056108–056116.
[21] J. Barre, A.R. Bishop, T. Lookman, A. Saxena, Physical Review Letters 94 (2005) 208701–208704.
[22] S. Bhosle, K. Gunasekera, P. Boolchand, M. Micoulaut, 2011, arXiv:1107.4768v1.
[23] H. He, M.F. Thorpe, Physical Review Letters 54 (1985) 2107–2110.
[24] K. Rompicharla, D.I. Novita, P. Chen, P. Boolchand, M. Micoulaut, W. Huff, Journal of Physics: Condensed Matter 20 (2008) 202101.
[25] T. Qu, D.G. Georgiev, P. Boolchand, M. Micoulaut, in: T. Egami, A.L. Greer, A. Inoue, S. Ranganathan (Eds.), Supercooled Liquids, Glass Transition and Bulk Metallic Glasses, Materials Research Society, 2003, p. 157.
[26] M. Micoulaut, Journal of Physics: Condensed Matter 22 (2010) 1–7.
[27] Y. Wang, P. Boolchand, M. Micoulaut, Europhysics Letters 52 (2000) 633–639.
[28] S. Stolen, T. Grande, H.-B. Johnsen, Physical Chemistry Chemical Physics 4 (2002) 3396–3399.
[29] R. Böhmer, C.A. Angell, Physical Review B 45 (1992) 10091.
[30] C.A. Angell, in: P. Boolchand (Ed.), Insulating and Semiconducting Glasses, World Scientific, Singapore, River Edge, NJ, 2000, pp. 1–51.
[31] M. Micoulaut, G.G. Naumis, Europhysics Letters 47 (1999) 568–574.
[32] F.J. Bermejo, C. Cabrillo, E. Bychkov, P. Fouquet, G. Ehlers, W. Häussler, D.L. Price, M.L. Saboungi, Physical Review Letters 100 (2008) 245902.
[33] J.C. Mauro, R.J. Loucks, Physical Review E 78 (2008) 021502.
[34] J.C. Mauro, American Ceram. Soc. Bull. 90A (2011) 31–37.